Conformal Printing of Electrically Small Antennas on Three-Dimensional Surfaces

Jacob J. Adams, Eric B. Duoss, Thomas F. Malkowski, Michael J. Motala, Bok Yeop Ahn, Ralph G. Nuzzo, Jennifer T. Bernhard, and Jennifer A. Lewis**

Increasingly stringent design constraints imposed by compact wireless devices for telecommunications, defense, and aerospace systems require the miniaturization of antennas. Unlike most electronic components, which benefit from decreased size, antennas suffer limitations in gain, efficiency, system range, and bandwidth when their size is reduced below a quarter-wavelength. The electrical size of the antenna is measured by its ka value, where k is the wavenumber ($k = 2\pi/\lambda$, λ = wavelength at the operating frequency) and a is the radius of the smallest sphere that circumscribes the antenna. Antennas are considered to be electrically small when $ka \leq 0.5$. Recent attention has been directed towards producing radiofrequency identification (RFID) antennas by screen-printing,[1] inkjet printing,[2] and liquid metal-filled microfluidics[3–5] in simple motifs, such as dipoles and loops. However, these fabrication techniques are limited in both spatial resolution and dimensionality; yielding planar antennas that occupy a large area relative to the achieved performance.

Omnidirectional printing of metallic nanoparticle inks offers an attractive alternative for meeting the demanding form factors of 3D electrically small antennas (ESAs). We have previously demonstrated that flexible, stretchable, and spanning silver microelectrodes with features as small as ~2 μm can be patterned both in and out-of-plane (e.g., spanning arches) on flat substrates by this approach.[6] Here, for the first time, we demonstrate the conformal printing of silver nanoparticle inks on curvilinear surfaces to create electrically conductive meander lines. When interconnected with a feed line and ground plane, the resulting 3D ESAs exhibit performance properties that nearly match those predicted theoretically for these optimized designs.

J. J. Adams,[+] Prof. J. T. Bernhard
Department of Electrical and Computer Engineering
University of Illinois at Urbana-Champaign
Urbana, IL 61801, USA
E-mail: jbernhar@illinois.edu
Dr. E. B. Duoss,[+,++] T. F. Malkowski,[+] Dr. B. Y. Ahn, Prof. J. A. Lewis
Department of Materials Science and Engineering
University of Illinois at Urbana-Champaign
Urbana, IL 61801 USA
E-mail: jalewis@illinois.edu
Dr. M. J. Motala, Prof. R. G. Nuzzo
Department of Chemistry
University of Illinois at Urbana-Champaign
Urbana, Illinois 61801, USA
[+] These authors contributed equally to this work.
[++] Present address: Lawrence Livermore National Laboratory, Center for Micro- and Nano- Technology, Livermore, CA 94550 USA

DOI: 10.1002/adma.201003734

Antennas act as effective transducers between free space and guided waves over a range of frequencies, known as their impedance bandwidth. The impedance of most small antennas can be approximated by a single resistor-inductor-capacitor (RLC) circuit, and their bandwidth is inversely proportional to their radiation quality factor (Q), defined as the ratio of energy stored to energy radiated.[7] Because of this inverse relationship, a low Q serves to increase bandwidth, and therefore the data rate over a given wireless channel. However, a fundamental relation exists between the antenna size and Q.[8,9] As the maximum dimension decreases below a wavelength, the bound on the minimum attainable Q rapidly increases, a phenomenon commonly referred to as Chu's limit – an important figure of merit for antenna performance. While Thal recently derived a more accurate bounding limit,[10] both limits depend on the electrical size of the antenna. For decades, researchers have sought antenna designs that approach these fundamental lower limits. However, prior efforts, such as those based on genetic algorithms[11,12] lack flexibility, since their output cannot be modified in a straightforward manner when design specifications change.

Our 3D electrically small antennas are fabricated by conformal printing of metallic inks onto convex and concave hemispherical surfaces in the form of conductive meander lines (**Figure 1**A). Their bandwidth approaches the fundamental limit for their size, offering nearly an order of magnitude improvement over rudimentary monopole antenna designs. With this approach, antennas can be rapidly adapted to new specifications, including other operating frequencies, device sizes, or encapsulated designs that offer enhanced mechanical robustness. Our ESA design is based on the fundamental principle that antennas filling a spherical volume most closely approach Chu's limit, thus yielding significant bandwidth improvements relative to their linear and planar counterparts.[13–15] This antenna, first constructed manually as a helical prototype[13] (Figure S1, Supporting Information), excites the fundamental transverse magnetic (TM_{10}) spherical mode, which has the lowest Q.[10]

To demonstrate our new design, we create four electrically small antennas (ESA1 – 4) of varying ka, operating frequency, and meander line size. Each antenna is constructed by conformal printing of a concentrated silver nanoparticle ink[6,16] in a digitally programmed meander line pattern onto either the exterior (convex) or interior (concave) surface of a hollow glass hemisphere. Unlike planar substrates, the surface normal is constantly changing on curvilinear surfaces, which presents added fabrication challenges. To conformally print features on hemispherical substrates, the silver ink must strongly wet

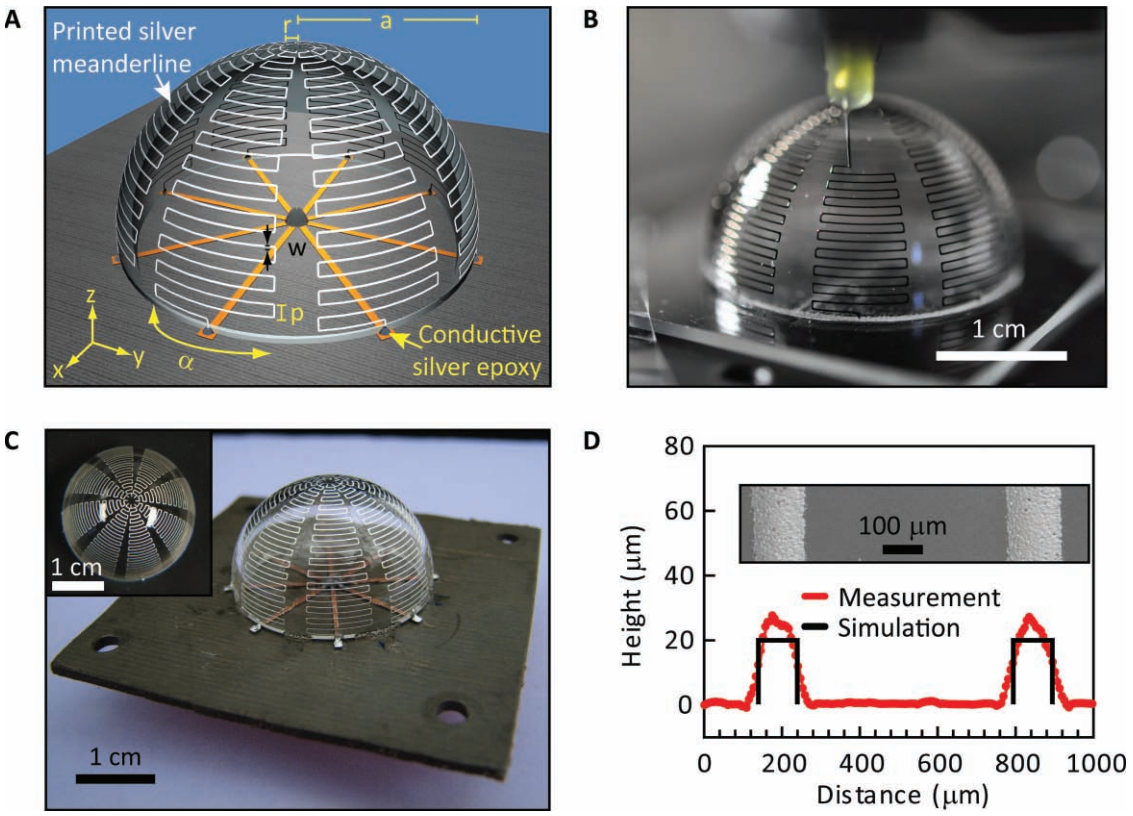

Figure 1. A) Schematic illustration of an electrically small antenna with labeled geometric parameters. B) Optical image of an antenna during the printing process. C) Optical images of a completed antenna (ESA1) in side and top (inset) views. D) Optical profilometry scan of representative meanderlines on ESA1 with the background surface subtracted and scanning electron microscopy image of these features (inset).

the surface to facilitate patterning even when the deposition nozzle (100 μm diameter) is perpendicular to surface normal (e.g., at the substrate base). In some cases, the nozzle is bent at an angle that ranges from 10–45° to further facilitate printing. For example, this modification is necessary when the nozzle diameter is reduced to 30 μm. After printing and annealing at 550 °C, the patterned meander lines exhibit an electrical resistivity of ~5×10^{-6} Ω·cm. Each antenna is then matched to have a 50 Ω impedance at the operating frequency, as previously reported.[13] The designs are simulated in a 3D full-wave electromagnetic field solver (HFSS, Ansoft Inc.) and their geometric parameters are summarized in Table S1 (Supporting Information). Note that the antenna's operating frequency is determined primarily by the printed conductor cross-section and the spacing (or pitch) between meander lines within each arm.

The antennas' impedance and radiation behavior are measured by a network analyzer. Using this method, the voltage standing wave ratio (VSWR) quantifies how well energy can be coupled from the source to the antenna. A VSWR of 1 indicates perfect coupling between source and antenna, while higher values of VSWR indicate increasingly poor coupling. The impedance bandwidth of the antenna is defined as the frequencies between which the VSWR is below a specified level. We measure the half-power bandwidth, a common figure of merit corresponding to a VSWR of 5.83 (see Experimental Section). Additionally, we measured the antenna's radiation efficiency, *i.e.*, the ratio of the radiated power to the total accepted power. The efficiency has an impact on the bandwidth, range, and fundamental limits, and its determination requires a Wheeler Cap measurement[17] (see Experimental Section). The electrical characteristics of each antenna are summarized in **Table 1**.

Figure 1B shows a representative antenna (ESA1) being patterned on the outer surface of the glass hemisphere; a video of this process is also provided (Video S1, Supporting

Table 1. Radiation characteristics of each antenna and their normalized Q values (measured Q divided by Chu and Thal limits).

Design	*ka*	Center Frequency [GHz]	Bandwidth	Efficiency	*Q*	Q/Q_{Chu}	Q/Q_{Thal}
ESA1	0.46	1.73	15.2%	71%	13.1	1.5	1.1
ESA2	0.21	0.79	6.3%	14%	31.9	2.0	1.4
ESA3	0.49	3.57	12.1%	63%	16.5	2.5	1.8
ESA4	0.45	1.70	12.6%	66%	15.9	1.8	1.4

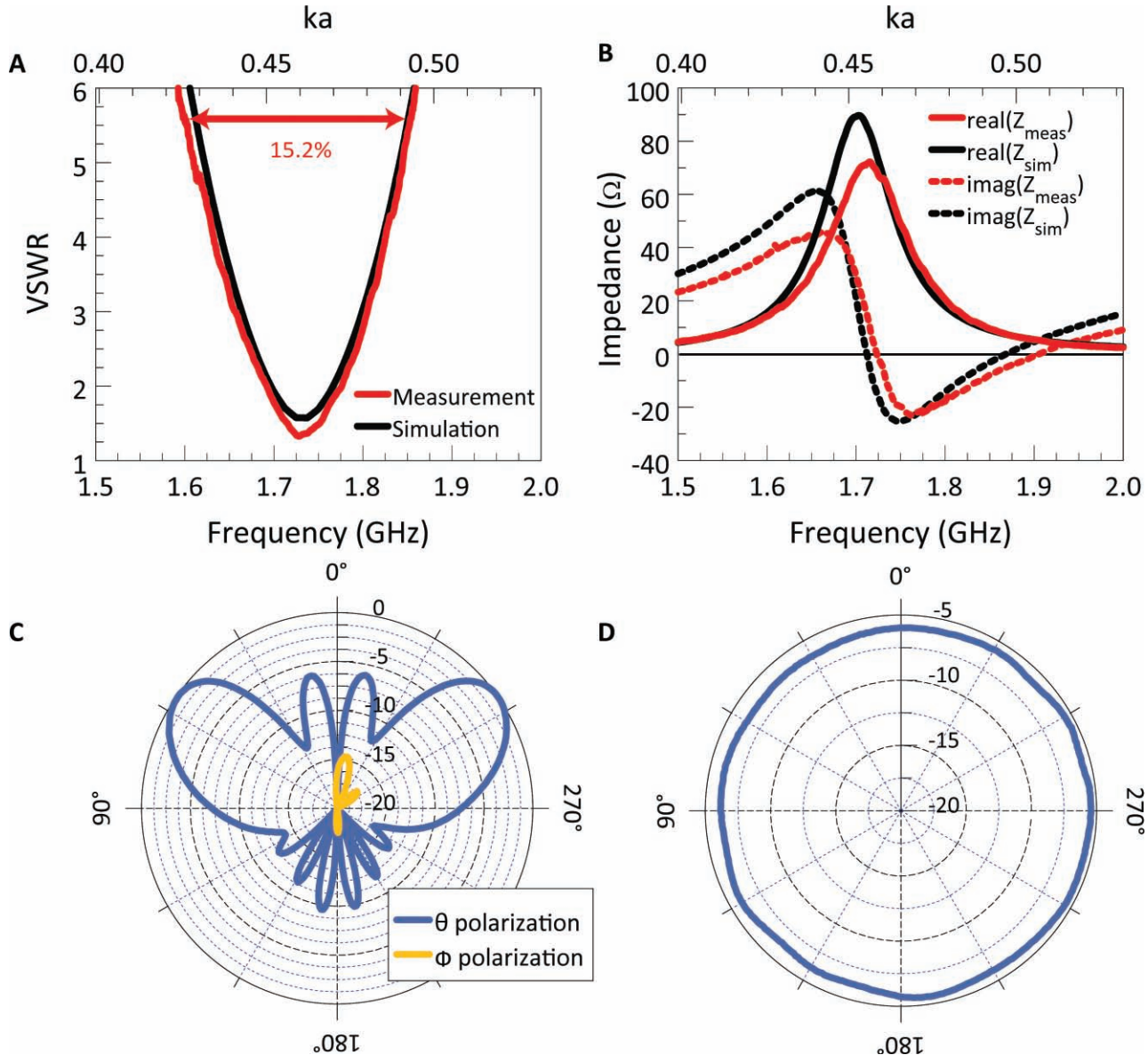

Figure 2. A) Measured and simulated VSWR versus frequency response for a representative antenna (ESA1). B) Measured and simulated impedance versus frequency response for this antenna. Normalized radiation pattern (dB) in C) elevation or *xz*-plane and D) in azimuth or *xy*-plane for this antenna.

Information). The printed antenna consists of tapered silver meander line "arms" that are affixed to patterned copper feed lines on a low-loss laminate substrate. An image of the completed antenna (ESA1), with a substrate radius of 12.7 mm, $ka \sim 0.5$, and a targeted operating frequency of 1.7 GHz, is shown in Figure 1C. In addition, 3D microcomputed tomography reconstruction is provided in Video S2 (Supporting Information). The cross-section of the printed meander lines is determined by an optical profilometry scan of two meander lines located ten horizontal arc segments from the base, shown in Figure 1D. The inset shows a scanning electron microscopy (SEM) image of these segments, which reveals the precise control of meander line width and spacing. We approximate the meander line cross-section by a 100 μm × 20 μm rectangle, which is used in the design simulations described above.

The VSWR characteristics and impedance measurements of a representative ESA1 are shown in **Figures 2**A and B, respectively. The antenna's measured center frequency is 1.73 GHz with a 5.83:1 bandwidth of 15.2%. To demonstrate the robustness and repeatability of this patterning technique, we printed multiple antennas with ESA1 parameters and acquired the VSWR data shown in Figure S2 (Supporting Information). The antennas' center frequencies range from 1.69 to 1.74 GHz, indicating that our fabrication process provides excellent control and reproducibility. The efficiencies of these antennas fall within the range of 68% to 72%, very close to the predicted value of 66%. Their efficiency, which is reasonable for an ESA of this size, is primarily affected by the resistivity of the meander line arms. We note that replacing them with copper, which has a three-fold lower resistivity, would only improve the

antenna efficiency by 5–10%. Applying the relation between Q and bandwidth,[7] we find that the antenna's Q is 13.1. This Q value is 1.5× the Chu limit and 1.1× the Thal limit, representing a greater than 50% improvement in performance relative to the helical antenna reported by Adams and Bernhard[13] and nearly an order of magnitude bandwidth increase compared to a conventional monopole design. Given that this antenna closely approaches the Thal limit, its design is essentially optimum for its size. For completeness, the antenna's radiation pattern is shown in Figures 2C,D. Importantly, we find that ESA1 exhibits excellent performance relative to the fundamental limits as well as good agreement with simulations.

Next, we demonstrate two approaches to tailoring the center operating frequencies of these electrically small antennas. In the first approach, we create an antenna (ESA2) with a smaller electrical size (ka ~ 0.2) by conformal printing of four conductive meander line arms on the convex surface of an identical glass hemisphere (a = 12.7 mm), targeting an operating frequency in the 700 MHz band. This spectrum is highly valued for mobile communications due to its propagation characteristics. In the second approach, we create an antenna (ESA3) of nominally the same ka ~ 0.5 on the convex surface of a smaller glass hemisphere (a = 6.55 mm), raising the targeted frequency to 3.6 GHz. In this case, the eight meander line arms are patterned by conformally printing the silver nanoparticle ink through a 30 μm nozzle to yield a three-fold reduction in their characteristic dimensions. Optical images of both antennas are provided in Figure S3 (Supporting Information) along with their measured VSWR values. The measured center frequency of ESA2 is 790 MHz with a 5.83:1 bandwidth of 6.3%, while its measured efficiency is 14%. This reduced efficiency is expected in antennas at smaller electrical sizes.[18] While the bandwidth is widened by the lower efficiency, no net effect is observed in the ratio of the antenna's Q to the Chu and Thal limits[7,19] (see Experimental Section). These ratios are slightly higher than the ESA1, because ESA2 only has four arms. As the number of arms increases, the radiating portion of the antenna more completely fills the spherical volume and exhibits a lower Q.[13] By contrast, ESA3 possesses Q ratios that are slightly higher than the other designs, because the thickness-to-diameter ratio of small glass hemisphere substrate is higher, and more energy is stored in this higher permittivity material than in air. The measured center frequency of ESA3 is nominally 3.6 GHz with a 5.83:1 bandwidth of 12.1%, while its measured efficiency is 63%.

To fabricate an antenna that can withstand mechanical handling, we conformally printed the fourth antenna (ESA4) on the interior surface of the glass hemisphere. The substrate is embedded in a PDMS mold to hold it in place during printing (**Figure 3**A); see Video S3 (Supporting Information) for a video of this process. After printing is completed, the patterned structure is removed from the mold. In this motif, the hollow glass hemisphere serves as a protective barrier, allowing the device to be easily handled and mounted on a low-loss laminate substrate (Figure 3B). Designed to perform nearly identically to ESA1, this antenna exhibits a Q close to the lower bound. The measured VSWR of ESA4 is shown in Figure 3C. Its center frequency is at 1.70 GHz with bandwidth and efficiency of 12.6% and 66%, respectively.

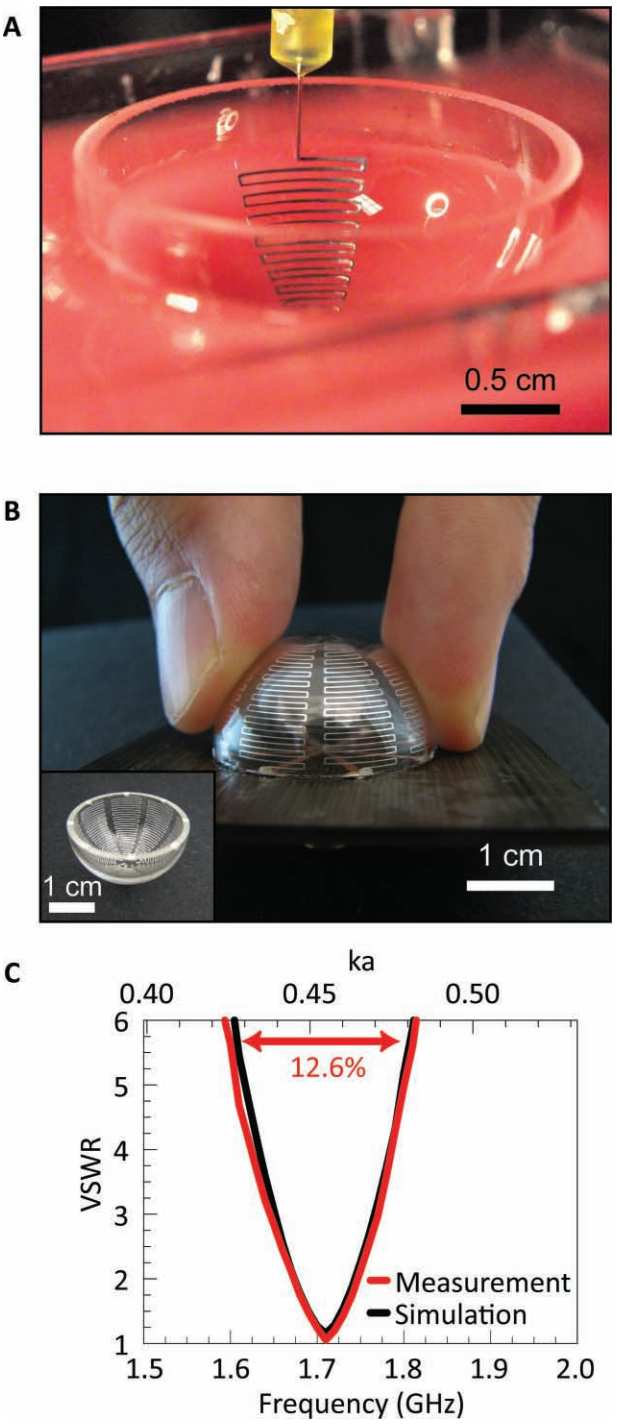

Figure 3. A) Optical image of an antenna (ESA4) being printed onto the interior surface of a glass substrate embedded in a PDMS mold. B) Optical images of this antenna before (inset) and after connecting to the feedlines. C) Measured and simulated VSWR versus frequency response.

In summary, we have demonstrated the conformal printing of 3D electrically small antennas, whose performance approaches the Chu limit. Our fundamental design approach enables specification of both operating frequency and size, while achieving near-optimal bandwidth at several frequencies of interest for

wireless communications. The ability to conformally print antennas that are compact and encapsulated within their support substrate further enhances their mechanical robustness. More broadly, conformal printing of conducting features may enable several applications, including flexible,[20,21] implantable[22] and wearable[23] antennas, electronics, and sensors.

Experimental Section

Ink preparation and hemisphere substrate alignment: Concentrated silver nanoparticle ink (~72 wt% silver)[6] is loaded into a micronozzle with inner diameter, d_{inner}, of 100 μm (Part 7018462, Nordson EFD) or 30 μm (pulled-glass capillary, P-2000, Sutter Instrument) and mounted onto a three-axis positioning stage with nanoscale resolution (positional accuracy = 50 nm, ABL 9000, Aerotech). The 1.2 mm thick glass hemisphere (Pyrex 7740, Ace Glass) is affixed to a glass slide, centered onto a precision rotation stage (sensitivity = 15 arc·s, M481-A, Newport), and secured to the stage. The hemisphere is aligned in the *xy*-plane to the nozzle by performing consecutive circular revolutions of radius = $a + d_{outer}$, where d_{outer} is the outer nozzle diameter, at the hemisphere base until minimal or no contact is made between the nozzle and hemisphere. Markers are printed onto the glass slide at intervals demarcating start points for each arm. A design file for the printing stage control program is generated with custom computer-aided design software by entering parameter values for a, d_{inner}, d_{outer}, the number of meander line arms, n, the angle each arm subtends at its base, α, the printed wire width, w, the pitch or center-to-center spacing within a meander line, p, the radius of the non-printed region at the hemisphere apex, r, and print speed, v. In this work, v ranged from 100–1000 μm s^{-1}.

Antenna fabrication: After substrate alignment, each antenna is conformally printed by loading and executing the design file as well as programming stop and start flow commands between meander line arms. In some cases, a bent micronozzle (bend angle = 10–45°) is used, which is loaded with ink, aligned to the markers and hemisphere, and a single arm is printed from a given start point. After finishing the arm and ceasing ink flow, the nozzle returns to the original start point, the hemisphere is precisely rotated to the next marker, and another arm is printed, continuing with additional arms in the same fashion. The approximate build time for a single antenna depends upon the design and print speed and ranges from roughly 30 min to 3 h. After printing, each antenna is heat treated to 550 °C in air for 3 h to form highly conductive silver traces.

Laminate substrate patterning and antenna attachment: The low-loss, copper-clad laminate substrate (Duroid 5880, Rogers Corp.) is patterned on one surface with a printed circuit board prototyping mill (Quick Circuit 5000, T-Tech Inc.) to create a feed line pattern. Next, a via is drilled through the feed line center and a 50 Ω SubMiniature version A (SMA) connector is affixed to the patterned feed line and ground surface with solder. Finally, the printed antenna is aligned with the copper feed lines and attached with nonconductive epoxy in the non-patterned regions. After curing, the meander lines are electrically connected to the feed lines with conductive silver epoxy. The completed antennas are characterized with an optical profilometer and scanning electron microscope.

Antenna measurements: Each antenna is secured to a copper ground plane (radius = 30 cm). Impedance measurements are taken using a vector network analyzer (E8363B, Agilent Technologies). After recording the free-space impedance characteristics of the antenna, a Wheeler cap is placed over the antenna and electrical connection to the ground plane is ensured. The Wheeler cap is a metallic box that shorts out the antenna's far-field radiation, enabling separate measurement of the radiation and loss mechanisms.[17] A variety of Wheeler cap sizes were used in this work to avoid cavity resonances that result in erroneous measurements in certain frequency ranges. Using the measurements from the Wheeler cap and free-space, the efficiency is calculated using methods from the literature.[17] Finally, the radiation pattern of the antenna is measured in the Illinois Wireless Wind Tunnel, an anechoic chamber that simulates infinite free-space. The antenna under test (AUT) is placed in the center of the chamber and a continuous-wave (CW) signal excites the antenna. The power radiated in one direction is measured by a standard gain horn antenna, and the AUT is rotated by a positioner to obtain a 360° radiation pattern.

Q calculations: The Chu and Thal limits are easily calculated once the *ka* value is known. The Chu limit[8,9] for a lossless antenna is related to *ka* as

$$Q_{Chu} = \frac{1}{ka} + \frac{1}{(ka)^3}$$

and the Thal limit is calculated from the Chu limit using tabulated values.[10] Q is reduced proportionally to radiation efficiency,[7] and so the Chu and Thal limits must be scaled by the efficiency.[19] Fractional bandwidth (FBW), defined as the absolute bandwidth divided by the center frequency and expressed as a percentage, is related to Q as

$$FBW = \frac{s-1}{Q\sqrt{s}}$$

where s is the VSWR at which the bandwidth is defined. Note that the half-power bandwidth is defined by the VSWR level 5.83 because the percentage of incident power that is reflected by the antenna is related to the VSWR by

$$\frac{P_r}{P_{inc}} = \frac{(s-1)^2}{(s+1)^2}$$

For half of the incident power to be reflected, $s = 5.828$.

Supporting Information

Supporting Information is available from the Wiley Online Library or from the author.

Acknowledgements

This research was supported by the US Department of Energy (DOE), Division of Materials Sciences, under award DE-FG02-07ER46471, through the Materials Research Laboratory (MRL). The materials characterization facilities were provided through the MRL Center for Microanalysis of Materials with support from the University of Illinois and DOE BES. The electromagnetic measurements were carried out at the Electromagnetics Laboratory using equipment supported through ARO DURIP grant DAAD 19-03-1-0112 and NSF CNS 04-23431. The Duroid substrates were provided by Rogers Corp. J.J.A. was supported by a National Science Foundation Graduate Research Fellowship. The authors thank J. Vericella, A. DeConinck, M. Bee, D. Stevenson, and A. Phillips for technical assistance and useful discussions. The authors also thank A. Jerez for help with the cover design.

Received: October 11, 2010
Revised: November 24, 2010
Published online: January 19, 2011

[1] D. Y. Shin, Y. Lee, C. H. Kim, *Thin Solid Films* **2009**, *517*, 6112.
[2] T. H. J. van Osch, J. Perelaer, A. W. M. de Laat, U. S. Schubert, *Adv. Mater.* **2008**, *20*, 343.
[3] M. Kubo, X. Li, C. Kim, M. Hashimoto, B. J. Wiley, D. Ham, G. M. Whitesides, *Adv. Mater.* **2010**, *22*, 2749.
[4] J.-H. So, J. Thelen, A. Qusba, G. J. Hayes, G. Lazzi, M. D. Dickey, *Adv. Funct. Mater.* **2009**, *19*, 3632.
[5] S. Cheng, A. Rydberg, K. Hjort, Z. Wu, *Appl. Phys. Lett.* **2009**, *94*, 144103.

[6] B. Y. Ahn, E. B. Duoss, M. J. Motala, X. Guo, S.-I. Park, Y. Xiong, J. Yoon, R. G. Nuzzo, J. A. Rogers, J. A. Lewis, *Science* **2009**, *323*, 1590.
[7] A. D. Yaghjian, S. R. Best, *IEEE Trans. Antennas Propag.* **2005**, *53*, 1298.
[8] L. J. Chu, *J. Appl. Phys.* **1948**, *19*, 1163.
[9] J. S. McLean, *IEEE Trans. Antennas Propag.* **1996**, *44*, 672.
[10] H. L. Thal, *IEEE Trans. Antennas Propag.* **2006**, *54*, 2757.
[11] H. Choo, R. L. Rogers, H. Ling, *IEEE Trans. Antennas Propag.* **2005**, *53*, 1038.
[12] A. Erentok, O. Sigmund, in *Proc. 2008 IEEE Int. Symp. Antennas Propag.*, **2008**.
[13] J. J. Adams, J. T. Bernhard, *IEEE Antennas Wireless Propag. Lett.* **2009**, *8*, 303.
[14] S. R. Best, *IEEE Trans. Antennas Propag* **2004**, *52*, 953.
[15] H. D. Foltz, J. S. McLean, in *Proc. 1999 IEEE Int. Symp. Antennas Propag.* **1999**, 2702.
[16] X. Guo, H. Li, B. Y. Ahn, E. B. Duoss, K. J. Hsia, J. A. Lewis, R. G. Nuzzo *Proc. Natl. Acad. Sci. USA* **2009**, *106*, 20149.
[17] M. Geissler, O. Litschke, D. Heberling, P. Waldow, I. Wolff, in *Proc. 2003 IEEE Int. Symp. Antennas Propag.* **2003**, 743.
[18] J. M. Gonzalez-Arbesu, S. Blanch, J. Romeu, *IEEE Antennas Wireless Propag. Lett.* **2003**, *2*, 147.
[19] S. R. Best, A. D. Yaghjian, *IEEE Antennas Wireless Propag. Lett.* **2004**, *3*, 314.
[20] S. R. Forrest, *Nature* **2004**, *428*, 911.
[21] Y. G. Sun, J. A. Rogers, *Adv. Mater.* **2007**, *19*, 1897.
[22] D.-H. Kim, J. Viventi, J. J. Amsden, J. Xiao, L. Vigeland, Y.-S. Kim, J. A. Blanco, B. Panilaitis, E. S. Frechette, D. Contreras, D. L. Kaplan, F. G. Omenetto, Y. Huang, K.-C. Hwang, M. R. Zakin, B. Litt, J. A. Rogers, *Nat. Mater.* **2010**, *9*, 511.
[23] M. Hamedi, R. Forchheimer, O. Inganas, *Nat. Mater.* **2007**, *6*, 357.